Reaction mechanisms of $C(^3P_J)$ and $C^+(^2P_J)$ with benzene in the interstellar medium from quantum mechanical molecular dynamics simulations

Mohammad Ebrahim Izadi

Department of Physical Chemistry, School of Chemistry,

College of Science, University of Tehran, Tehran, Iran

Kristof M. Bal*

Department of Chemistry, Research Group PLASMANT, NANOlab Center of Excellence, University of Antwerp,

Universiteitsplein 1, 2610 Antwerp, Belgium

Ali Maghari

Department of Physical Chemistry, School of Chemistry,

College of Science, University of Tehran, Tehran, Iran

Erik C. Neyts

Department of Chemistry, Research Group PLASMANT, NANOlab Center of Excellence, University of Antwerp,

Universiteitsplein 1, 2610 Antwerp, Belgium

While spectroscopic data on small hydrocarbon in the interstellar medium in combination with crossed molecular beam (CMB) experiments have provided a wealth of data on astrochemically relevant species, much of the underlying mechanistic pathways of their formation remain elusive. Therefore, in this work, the chemical reaction mechanisms of $C(^3P_J)$ + C_6H_6 and $C^+(^2P_J)$ + C_6H_6 systems using quantum mechanical molecular dynamics (QMMD) technique at the PBE0-D3(BJ) level of theory is investigated, mimicking a CMB experiment. Both the dynamics of the reactions as well as the electronic structure for the purpose of the reaction network are evaluated. The method is validated for the first reaction by comparison to the available experimental data. The reaction scheme for the $C(^3P_J)$ + C_6H_6 system covers the literature data, e.g. the major products are 1,2-didehydrocycloheptatrienyl radical (C_7H_5) and benzocyclopropenyl radical (C_6H_5-CH), and it reveals the existence of less common pathways for the first time. The chemistry of the $C^+(^2P_J)$ + C_6H_6 system is found to be much richer, and we have found that this is because of more exothermic reactions in this system in comparison to $C(^3P_J)$ + C_6H_6 system. Moreover, using the QMMD simulation, a wealth of reaction paths have been revealed

that produce three distinct classes of reaction products with different ring sizes. All in all, at all the collision energies and orientations, the major product is the heptagon molecular ion for the ionic system. It is also revealed that the collision orientation has a dominant effect on the reaction products in both systems, while the collision energy mostly affects the charged system. These simulations both prove the applicability of this approach to simulate crossed molecular beams, and provide fundamental information on reactions relevant for the interstellar medium.

I. INTRODUCTION

Polycyclic aromatic hydrocarbons (PAHs) have drawn much attention from astronomers,[1, 2] astrobiologists,[3] and the combustion community.[4] About 18% of cosmic carbon is proposed to be in the form of PAHs. These species are believed to be formed in the outflow of dying carbon-rich stars and they can protect the inner environments from the destructive radiation fields. Moreover, aromatic molecules as well as carbonaceous nanoparticles play an essential role in catalyzing molecular hydrogen formation in the interstellar space. In spite of the pivotal importance of PAHs, the reaction pathways of the very first building block of this type of compounds, benzene, with C/C^+ atoms/ions remain unclear in some aspects. Benzene has been suggested to be the primary aromatic molecule involved in the formation of PAHs.[5-8]

Physical conditions in the interstellar medium (ISM) are not stable and change widely, e.g. ranging from very tiny hot plasmas to dense clouds of extremely cold gas. There are different phases of the ISM (each with their own characteristics) including: (a) the hot ionized regions with extraordinarily low density and high temperature, $n \approx 10^{-3}$ cm^{-3} and $T \approx 10^6$ K, respectively. In this local, there remains a very hot plasma containing atomic ions such as C^{3+} and O^{5+}; (b) the warm ionized medium which has low density and warm temperature, $n \approx 0.1$ cm^{-3} and $T \approx 8000$ K, respectively, and it contain partially ionized gases; (c) the warm neutral area having low density of about 0.5 cm^{-3}, warm temperature around 8000 K and neutral gases; (d) the cold neutral zone having moderate density and cool temperature, $n \approx 50$ cm^{-3} and $T \approx 100$ K, respectively. This area is often known as diffuse atomic clouds in which hydrogen is mainly in the atomic form and also there remain neutral gases; (e) molecular clouds having generally moderate-to-high density and cool-to-cold temperature separating into diffuse molecular clouds and dense molecular clouds, $n \approx 100$ to $> 10^4$ cm^{-3} and $T \approx 70$ to < 30 K, respectively. In molecular clouds, hydrogen is predominantly in molecular form, H_2. Diffuse molecular clouds are relatively transparent to ultraviolet (UV) photons while dense molecular clouds are opaque to UV photons.[9-12] Therefore, in outer space, formation of the interstellar molecules mostly depends on the medium in which the atoms interact. For example, in low density regions where the cosmic rays or radiations may produce ions/radicals form neutral species, interstellar molecules are mostly formed by binary, 2-body, neutral-neutral reactions involving radical species or ion-neutral gas-phase reactions. In addition, in this area, ternary, 3-body, reactions may not be important because of the low gas densities.[12-14]

Crossed molecular beam (CMB) experiments are the most versatile technique in the investigation of primary 2-body reactions under a single collision condition. This technique contains the reactants in separate beams, in well-defined quantum states and at specific collision energy impacting in the single collision condition. These characteristics supply a unique approach to follow the consequences of a single collision event, avoiding secondary collisions and wall effects. Several studies has already been undertaken on CMB experiments supported by electronic structure calculations to investigate mechanisms of the chemical reactions related to astrophysics.[15-20]

In recent years, there has been an increasing interest in utilizing computational methods, specifically density functional theory (DFT) and quantum mechanical molecular dynamics (QMMD) simulations,[21-24] to unravel chemical reaction mechanisms and construct accurate reaction networks.[25-27] However, according to the best of our knowledge, no QMMD simulations of astrochemically relevant CMB experiments were carried out so far. To be precise, several studies have combined CMB experiments and electronic structure computations to study the reactions mechanisms of C_2 in the $^1\sum_g^+$ ground state and ethylene (C_2H_4),[28] allyl radicals (C_3H_5 (X^2A_2)) with two C_3H_4 isomers, methyl-acetylene (CH_3CCH (X^1A_1)) and allene (H_2CCCH_2 (X^1A_1)),[29] carbon in the ground state (^3P_j) and 1,3-butadiene ($H_2CCHCHCH_2$),[15] phenyl radicals (C_6H_5) with isoprene ($CH_2C(CH_3)CHCH_2$) and 1,3-pentadiene ($CH_2CHCHCHCH_3$).[30] For all of these systems, a theoretical potential energy surface (PES) and reaction network was proposed, but only on the basis of "static" QM calculations: no dynamic simulations at a QM level of theory (i.e., QMMD) were performed. Additionally, a series of reaction mechanisms were suggested for $C(^3P_J)$ + C_6H_6 using CMB experiments based on experimental investigations supported by electronic structure calculations. Although these efforts lead to a reaction scheme of this system reported in the literature,[16, 31, 32] explicit probing of the reaction process with QMMD simulation may provide additional insights with less ambiguity and bridge the gap between explicitly dynamic experiments and detailed quantum chemical calculations. Moreover, due to the relatively large quantity of carbon in the interstellar medium and since the ionization energy of atomic carbon is smaller than that of atomic hydrogen, C^+ is believed to be one of the principal ions in diffuse clouds. Therefore much of the ion chemistry is believed to start with C^+.[33] Although some mass spectroscopy investigations were performed to elucidate mechanisms of chemical reactions of $C^+(^2P_J)$ with C_6H_6[34, 35] the reactions of this system have not yet been studied in depth. In addition to the essential importance of atomic ion reactions, it is also of interest to understand the differences between reactions of C^+ ions and corresponding reactions of C atoms. Therefore, the purpose of this study is to explicitly simulate CMB experiments of $C(^3P_J)$ and $C^+(^2P_J)$ interacting with benzene using QMMD. Intermediates, transition states and products observed in the simulations will then be further characterized using static electronic structure calculations to construct a reaction network for each system.

II. COMPUTATIONAL METHODOLOGY

A. Crossed molecular beam simulation using QMMD method

1. Simulation of the crossed molecular beam

The crossed molecular beam (CMB) reactions of $C(^3P_J)$ and $C^+(^2P_J)$ with benzene were conducted at collision energies of 2.1 kcal mol^{-1} (Carbon velocity = V_C= 1220 & Benzene velocity = V_B= 440 m s^{-1}, lowest), 7.6 kcal mol^{-1} (V_C= 2350 & V_B= 770 m s^{-1}, medium) and 12.4 kcal mol^{-1} (V_C= 3067 & V_B= 770 m s^{-1}, highest) under single collision conditions. The simulations are performed in two steps, viz. a thermalization stage and a collision stage. In the thermalization stage, a benzene molecule is thermalized in the canonical ensemble at 300 K for 1 ps (0.25 fs time step). The temperature was controlled by a Nosé-Hoover chain thermostat using a temperature damping constant of 25 fs. In the subsequent collision stage, all simulations were carried out in the microcanonical ensemble for 2 ps with a time step of 0.25 fs. During the thermalization stage, the atomic velocities of the system were saved every 100 steps. Initial conditions for the collision stage at each collision energy were then chosen from 10 such states recorded between the 3100^{th} the 4000^{th} step, to have a statistically independent starting configurations and atomic velocities for the benzene molecule. The number of repeats per condition is fairly low, which is a consequence of the rather expensive hybrid DFT level of theory we have chosen to employ. However, as can be seen in Table S1 in the supporting information, doubling the number of simulations does not appreciably affect the sample of observed mechanisms. Our QMMD simulations will thus be able to provide sufficient information for an initial mechanistic analysis.

It should be noted that the thermalization stage only concerns the internal degrees of freedom of the benzene molecule; the relative velocities of the benzene molecule and carbon atom/ion are always fixed at one of the abovementioned values. The physical significance of this procedure is that it accounts for the fact that even if all collisions in the beam occur at the same impact energy, differences in the benzene's orientation, rotational energy, and vibrational energy can still yield different reaction outcomes. Therefore, the simulated temperature of 300 K is merely intended to generate a reasonable distribution over atomic configurations and momenta. While this is computationally efficient, we acknowledge that in the supersonic expansion the molecules have in fact a very low (~10 K) rotational and vibrational temperature,[36-41] which is not captured in our simulations. Indeed, our QMMD simulations treat nuclei classically and imply equipartition, which would mean that atoms will barely move from their equilibrium positions at such a low temperature. In reality, nuclear quantum effects (NQEs), more specifically zero point vibration, will generate a broader distribution of equilibrium configurations and do not distribute energy equally over all modes. As a result, in the framework our classical molecular dynamics simulations ("classical" in the sense that nuclei motion is treated classically), thermalization at some elevated temperature is our best attempt to capture the configurational distribution arising from zero point motion. Accounting for NQEs more rigorously, for example by path integral MD or approximations thereof,[42] may therefore be an interesting avenue for

future research. Although it would be very difficult to find a region exactly with this temperature within the ISM (which varies between less than 30 K to 10^6 K), the conditions considered in this study may be similar to the proto–planetary nebula CRL 618.[43, 44]

Compared to CMB studies, one additional degree of freedom is explicitly investigated, namely, the orientation of benzene molecule: the C^+/C atom was allowed to collide with the benzene ring through face, edge-in-plane and edge-out-of-plane orientations at each collision energy. This ability to disentangle different collision orientations is one of the advantages offered by QMMD simulations that is not accessible from either CMB experiments or from static QM calculations. As summarized in Table 1, in total 180 simulations were performed for two different chemical systems with various orientations, collision energies and initial random velocities. It should be noted that while we use CMB experiments as an inspiration for our simulation setup and as a way to compare reaction products, an exact recovering of reaction of the full experimental results such as angular and translational energy distributions is computationally prohibitive and outside the scope of this study. The admittedly limited sample size of our simulations did, however, prove to yield a sufficiently complete set of reaction pathways, products, and intermediates.

To put the reactants in the same initial positions all setups are based on the center of mass of benzene (COMB). After evaluation of the COMB, the distance b between the collision center and the COMB is determined. Practically, by considering b=1.5 Å (face collisions) or b=2.9 Å (edge collisions) as a distance between the COMB and collision center only in collision direction, the location of the collision center is calculated (Fig. 1). Thus, we introduce the b parameter to ensure the same configuration of fragments upon impact. We assume that the atom and molecule fully interact by van der Waals forces within this distance. In the edge collision cases, b is composed of two components, viz. 1.5 Å for van der Waals interactions and 1.4 Å for the benzene radius in the plane. For all cases, C^+/C and benzene were positioned at least 5 Å from each other in the initial position, and the beams approach each other in 90^o similar to experimental setups in CMB experiments.

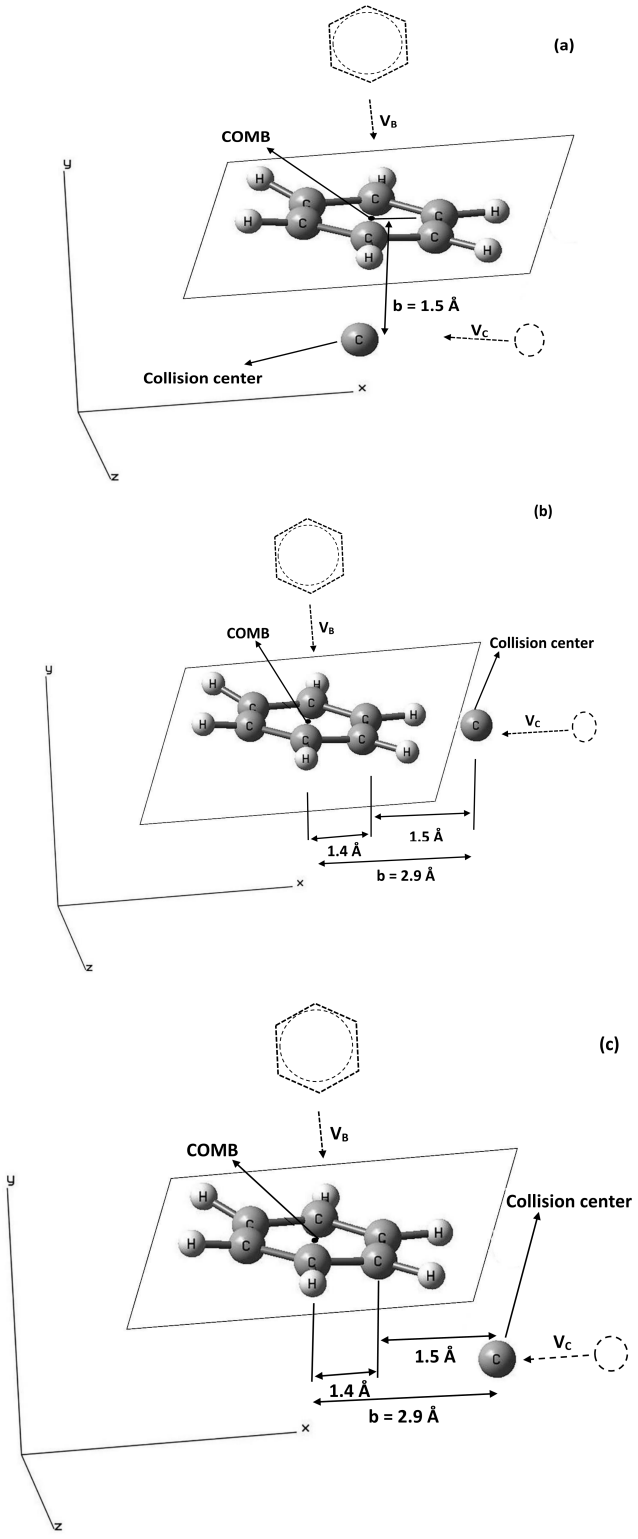

Fig. 1 Schematic representation of the configurations of all simulations at the collision moment for face (a), edge in-plane (b) and edge out-of-plane (c) orientations.

Table 1. Summary of the all the different CMB simulations that were carried out in this work. Different collision energies (E_C), velocities of carbon and benzene (V_c and V_B) and collision orientations were used for both systems.

E_c, kcal mol^{-1}	V_B, m/s	V_C, m/s	Collision orientation	System
2.1	440	1220	Face In-plane Out-of-plane	$C(^3P_j) + C_6H_6$ $C^+(^2P_j) + C_6H_6$
7.6	770	2350	Face In-plane Out-of-plane	$C(^3P_j) + C_6H_6$ $C^+(^2P_j) + C_6H_6$
12.4	770	3067	Face In-plane Out-of-plane	$C(^3P_j) + C_6H_6$ $C^+(^2P_j) + C_6H_6$

2. QMMD simulations

We performed quantum mechanical molecular dynamics (QMMD) simulations within the Born-Oppenheimer approximation as implemented within the CP2K program package, i.e., with explicit treatment of the valence electrons in the system.[21, 24, 45] All simulations were carried out within the Gaussian and plane wave (GPW) formalism,[46] employing Goedecker-Teter-Hutter (GTH) pseudopotentials to describe the core-valence interactions and a polarized triple-ζ (m-TZV2PX) basis set to expand the Kohn-Sham valence orbitals.[23, 47, 48] An auxiliary plane wave basis set was used to expand the electron density, defined by a cutoff of 400 Ry. A periodic simulation cell was used to avoid boundary artifacts.

Because the overall trajectories and system evolutions in our energy-conserving simulations are strongly dependent on the energy release from bond formation reactions occurring upon impact, it is crucial to describe the thermochemistry accurately. For this reason, we opted to use a hybrid DFT functional (PBE0, with 25% Hartree-Fock (HF) exchange),[49, 50] supplemented by Grimme's D3 dispersion correction in its Becke-Johnson damping form.[51, 52] The resulting PBE0-D3(BJ) level of theory has thermochemical errors that are only about half[53] of its dispersion-uncorrected parent GGA functional PBE[54] and was recently shown to be one of the most transferable DFT methods.[55] This particular choice of functional should therefore introduce only a reasonably small method-induced bias to our conclusions. Moreover, hybrid functionals offer a more accurate description of reaction barriers. A disadvantage of using a hybrid functional in QMMD simulations over GGA is the high cost of

evaluating the exact exchange term. In CP2K, such computations can be made feasible by the auxiliary density matrix method (ADMM),[56] in which we employ a small uncontracted polarized triple-ζ (pFIT3) basis to evaluate the exchange integrals. The HF term was truncated at 5 Å.

B. QM calculations

All products, intermediates, and transition states observed over the QMMD simulations were further analyzed in more detail through all-electron calculations in Gaussian 16.[57] For consistency with the QMMD simulations, we employed the same PBE0-D3(BJ) level of theory and a basis set of roughly similar size and structure, i.e., Dunning's augmented correlation-consistent polarized valence basis set aug-cc-pVTZ.[58] Transition states were found using the Berny algorithm,[59] optimizing the structure to a saddle point rather than a local minimum. Zero point vibrational corrections to the energy (ZVPE) were consistently applied. The structures and energies obtained in these calculations are those that are reported in the discussion.

III. RESULTS AND DISCUSSIONS

To unravel the precise mechanisms of the elementary reactions of benzene with $C^+(^2P_J)$/$C(^3P_J)$ ions/atoms three different collision energies in three orientations were investigated dynamically using QMMD, supported by static electronic structure calculations. In the dynamic part, major products and different pathways could be explicitly tracked for the different conditions. Then, using the same level of theory, electronic structure calculations were performed to re-optimize all structures observed in the QMMD simulations, in order to create a reaction scheme.

A. $C(^3P_j)$ + C_6H_6 reaction

Fig. 2(a-c) shows the effect of orientation and collision energy on the products of the CMB simulations of $C(^3P_J)$ with C_6H_6 after 2 ps. According to the literature,[16] the reactions in the $C(^3P_J)$ + C_6H_6 system proceed mainly through a triplet mechanism rather than singlet. Intersystem crossing from triplet to singlet occurs only very rarely, and therefore we decided to explore the reaction network solely on the triplet surface as shown in Fig. 3. In this Figure all energies were calculated using PBE0-D3(BJ)/aug-cc-pVTZ level of theory and also ZPVE corrections are included. Moreover, to compare with the literature alternative energies from Ref. 12 are given in brackets.

As shown in Fig. 2(b), face collisions mainly produce C_7H_6 (P6 in Fig. 2(a)) while edge in-plane collisions are mostly producing C_6H_5-CH (P4 in Fig. 2(a)); however, there is no significant selectivity on edge out-of-plane collisions. According to the trajectories, once $C(^3P_J)$ and C_6H_6 are close they may interact in two ways, repulsion or attraction. In some edge in-plane collisions repulsion arises between the H atom and the approaching carbon, leading to a rotation of benzene and then a secondary (possibly reactive) impact occurs, approaching in a different orientation. In particular, all of the C_7H_6 products

(P6 in Fig. 2(a)) in edge in-plane orientation resulted from this mechanism (Fig. 2(b)). A repulsive interaction occurs when $C(^3P_J)$ approaches exactly at the COM of benzene, in this study for all face orientations. In these cases carbon will change its direction towards a C-C bond or the C atom of benzene resulting in C insertion (the carbon atom first adds to the π-system of the benzene molecule as part of a metastable three-membered ring, after which this ring opens to produce a heptagon (Fig. 3)), C_7H_6 (P6), or ejecting a C-H group, C_6H_6-CH (P4), respectively. The three C_6H_6-CH molecules produced in face collisions were produced by ejecting a C-H group (Fig. 2(b)). In edge out-of-plane collisions there were mostly attractive interactions resulting in both C_6H_6-CH and C_7H_6 mainly by C-H or C insertions, respectively. However, in a few collisions, ejecting the C-H group also was observed. In fact, in edge out-of-plane impacts, atomic carbon and benzene would pass each other if they wouldn't interact, but the attractive interaction between the π-system of benzene and the electrophilic nature of $C(^3P_J)$ induces collisions anyway, and the type of collision seems to more or less random yield both C_6H_6-CH and C_7H_6 with roughly the same possibility.

Fig. 2(c) suggests that different collision energies do not have a considerable effect on the type of products. However, by searching within the trajectories, at higher collision energies it was observed that the intermediates had a much shorter lifetime and are immediately converted to the products. For example, at the highest collision energy R → P1 → TS6 → P6 and R → P5 → TS5 → P4 pathways in Fig. 3 are proceeding extremely fast. Thus, they can be considered as direct insertions of C in C-C and C-H bonds, respectively. On the other hand, only at lowest energy one of the trajectories led to the P2 intermediate. As a result, different collisions energies may change the lifetime of the intermediates, although they do not have a significant effect on the type of the products. Over all of the simulations, all collision energies and orientations of this system, only one of two final products is observed.

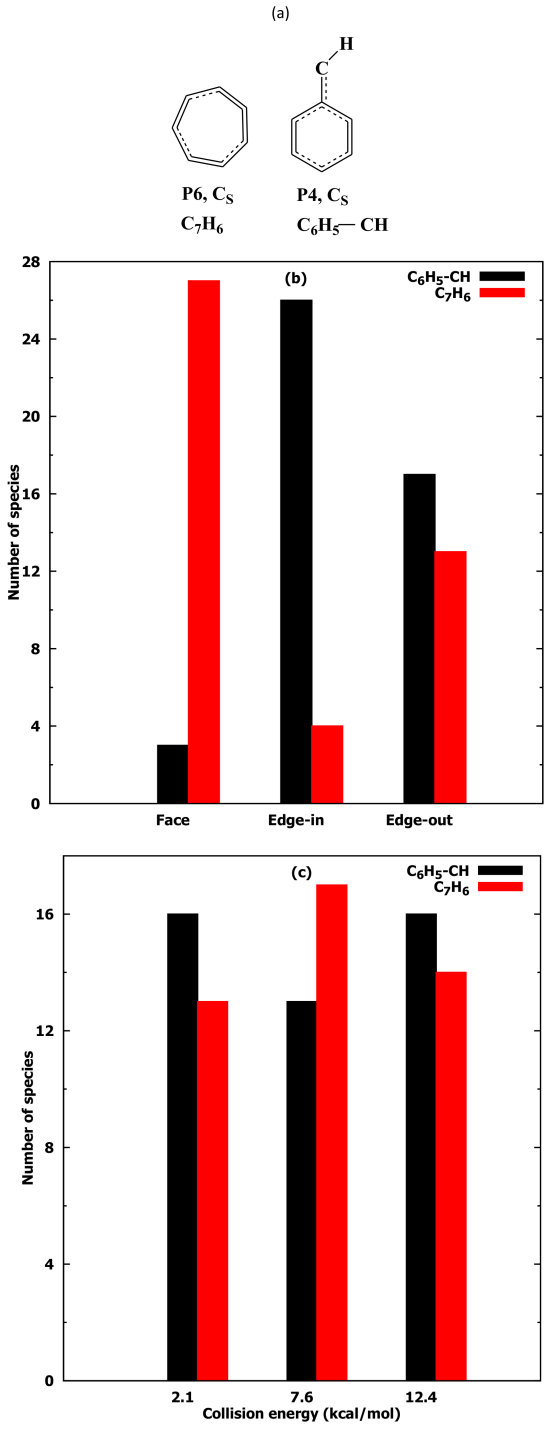

Fig. 2 Number/type of products (a) resulting from CMB simulations of the $C(^3P_J)$ + C_6H_6 system versus different approaching directions (b) and collision energies (c) after 2 ps NVE QMMD simulation.

1. Reaction scheme of $C(^3P_J) + C_6H_6$ system

The reaction network of $C(^3P_J) + C_6H_6$ system, Fig. 3, shows carbon atom addition to the π-system of benzene can occur barrierlessly, producing a weakly stabilized intermediate P1. Subsequently, P1 isomerizes to P6 by passing an extremely small barrier of only 0.6 kcal mol^{-1}, TS6. This low-barrier pathway, R → P1 → TS6→ P6, is exactly the same path reported previously in the literature.[16] Moreover, we observed two additional low-barrier pathways. First, the production of P4 in the dynamic simulations mostly proceeds through a fairly high lying transition state TS5, which is the most likely path to the C_6H_5-C-H structure, although the likely intermediate P1 was not clearly distinguishable. For more details on the dynamics of this pathway a video is provided in the supporting information. Second, in a few cases, especially at higher collision energies the impinging carbon atom directly ejects a C-H group out and produces the P2 intermediate, and subsequently P2 isomerizes to P4 or P6. By investigating the trajectories of the simulations, the weight of each route was obtained as reported in Table 2. As can be seen in this Table, P4 and P6 are mainly producing through R → P1→ P4 and R → P1 → P6, respectively.

Table 2. Percentage of each pathway over the 90 CMB simulations of $C(^3P_J) + C_6H_6$ system.

Pathway	Percentage
R → P1 → P4	44
R → P1 → P2 → → P4 or P6 R → P2 → → P4 or P6	7
R → P1 → P6	49

Somewhat surprisingly, the pathway through P5, which has to pass the high-lying state TS5, is more prevalent than the pathway along intermediates P1 and P2, passing the lower (by 8.8 kcal/mol) TS1. In combination with the lack of explicit observations of a P1→ P5 transition, and the very limited effect of the impact energy, we have to question the relevancy of interpreting pathways purely through the lens of activation energies. Indeed, the very large energy release upon formation of P1 will likely supply enough energy to cross any barrier almost instantly (as evidenced by our ability to observe reactions in each of our 2 ps simulations). This suggests that selectivity will be mostly driven by geometric arguments, i.e., the initial orientation of the benzene molecule upon impact, which is indeed what we see in Fig. 2(b). Even before P1 is fully formed (which is exothermic by 25.4 kcal/mol), enough heat will have been released to cross any of the here identified transition states, the most likely of which depending on the instantaneous location of the incoming C atom. Face impacts will therefore favor formation of P1, whereas in plane collisions can directly lead to TS5 without explicitly having to pass through P1.

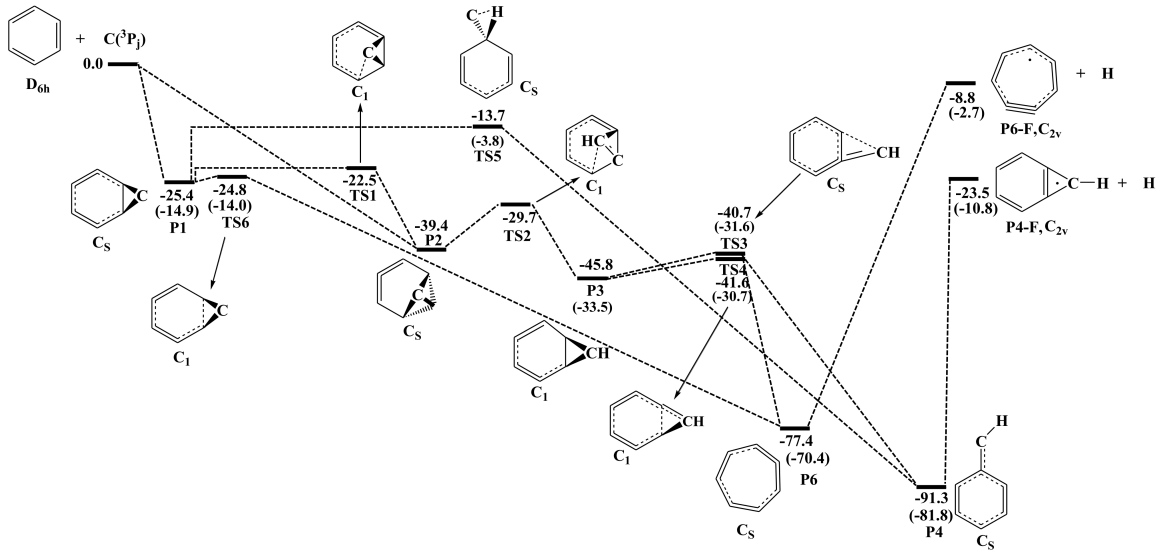

Fig. 3 Schematic representation of reaction pathways of $C(^3P_J) + C_6H_6$ system for the triplet state using PBE0-D3(BJ)/aug-cc-pVTZ + ZPVE (PBE0-D3(BJ)/aug-cc-pVTZ) level of theory. Relative energies are provided in kcal mol^{-1} and for some cases alternative energies from literature[16] are given in brackets.

As shown in Fig. 3, the relative energies obtained in this study are about 10 kcal mol^{-1} below the energies reported in Ref. 12 (the data in brackets). In Ref. 12 the authors employed the B3LYP/6-311+G** level of theory, while in this study we have used the PBE0-D3(BJ)/aug-cc-pVTZ level of theory. So, not only are the functional and basis set different but in our work, dispersion corrections are also included. According to recent benchmarks,[53] on a series of Diels-Alder reaction energies, B3LYP and B3LYP-D3(BJ) underbind by 15.75 and 8.03 kcal mol^{-1}, respectively, while PBE0 underbinds by only 0.45 kcal mol^{-1} and PBE0-D3(BJ) overbinds by -3.76 kcal mol^{-1}. In addition, for a test set with bond separations in alkanes, B3LYP underbinds by -10.70 kcal mol^{-1} and dispersion mostly cures this to -3.35 kcal mol^{-1} for B3LYP-D3(BJ), alternatively PBE0 also underbinds but a little less, -7.59 kcal mol^{-1}, and dispersion similarly cures this to -3.25 kcal mol^{-1} for PBE0-D3(BJ). As a result, the first set shows systematic problems of B3LYP for C-C bond formation, and the second set shows dispersion corrections are always needed regardless of functional characteristics. Therefore, it is concluded that B3LYP without dispersion corrections always underestimates C-C bond energies, which is in line with the comparison between this study and Ref. 12, and that PBE0-D3(BJ) is likely the more reliable method for this system. Note, also, that an accurate description of heats of reaction is crucial in the QMMD simulation, because the magnitude of the released heat controls much of the chemistry.

B. $C^+(^2P_j) + C_6H_6$ reaction

In the $C^+(^2P_j) + C_6H_6$ system, there exist several intermediates that may undergo different isomerizations through ring-opening and closure and multiple hydrogen migration steps. Therefore, to simplify the analysis of the paths and products the pathways/products are grouped based on the largest ring within the intermediates. All reactions are divided into three channels: those producing pentagon, hexagon or heptagon isomers, respectively. Accordingly, in Fig. 4, the effect of orientation and collision energy on formation of each series of isomers are depicted. In this Figure all data was extracted from the QMMD simulations of CMB reactions after 2 ps simulation. In addition, to draw the reaction pathways for this system, all structures observed during the simulations were optimized at the PBE0-D3(BJ)/aug-cc-pVTZ level of theory, including ZPVE corrections. This results in the reaction network shown in Fig. 5. Clearly, the reaction network is quite intricate, making it difficult to put all details in a single graph. As a result, the total reaction scheme in Fig. 5 was divided into separate schemes focusing on pentagon, hexagon and heptagon products in Fig. 6, Fig. 7 and Fig. 8, respectively.

1. Orientation and collision energy effects

According to the distribution of the QMMD products shown in Fig. 4(a), face collisions mostly generate heptagons while most pentagons are the result of edge collisions. Although both types of edge collisions have an equal probability of generating pentagons and heptagons, the likelihood of forming hexagons in edge out-of-plane collisions is higher. On edge in-plane collisions there is one main interaction: repulsion between H atom and C^+ leading to the rotation of benzene, after which C^+ approaches from a new direction and in which C^+ is strongly attracted by the π electrons. Afterward, C^+ may either collide with a carbon atom of the ring (Com-2 pathway in Fig. 5) and mainly produce a heptagon, insert into a C-C bond directly so as to produce a heptagon (Com-1 pathway), or eject two CH groups yielding pentagon-containing polycyclic structures (Com-0 pathway). Edge out-of-plane and edge in-plane collisions mostly proceed through more or less similar heptagon and pentagon production pathways because almost all of the edge in-plane impacts result in a rotation of the benzene ring and in this case the orientations become similar to the edge out-of-plane impacts. The significant difference between Com-1 and Com-2 is the lifetime during the dynamic conversion: Com-1 has a very short lifetime as if the reaction proceeds instantaneously, while Com-2 takes longer time to convert to P2.

As shown in Fig. 4(b), the production of a heptagon is dominant at collision energies of 2.1 kcal mol^{-1}, more so than at 7.6 and 12.4 kcal mol^{-1}. This behavior is due to the pathway which proceeds through Com-2. This pathway is the most likely route in the production of heptagons at the lowest energy (according to the trajectories, 9 cases out of 17 are produced through Com-2, while there are 7 paths in total, Fig. 5 and Fig. 4(b)). Although two possible barriers can be crossed (TS13 & TS12), they have both a very low height and also Com-2 is more stable than Com-1 (Fig. 8). Just like the collisions of the neutral C atom, however, the overall effect of the collision energy is quite small.

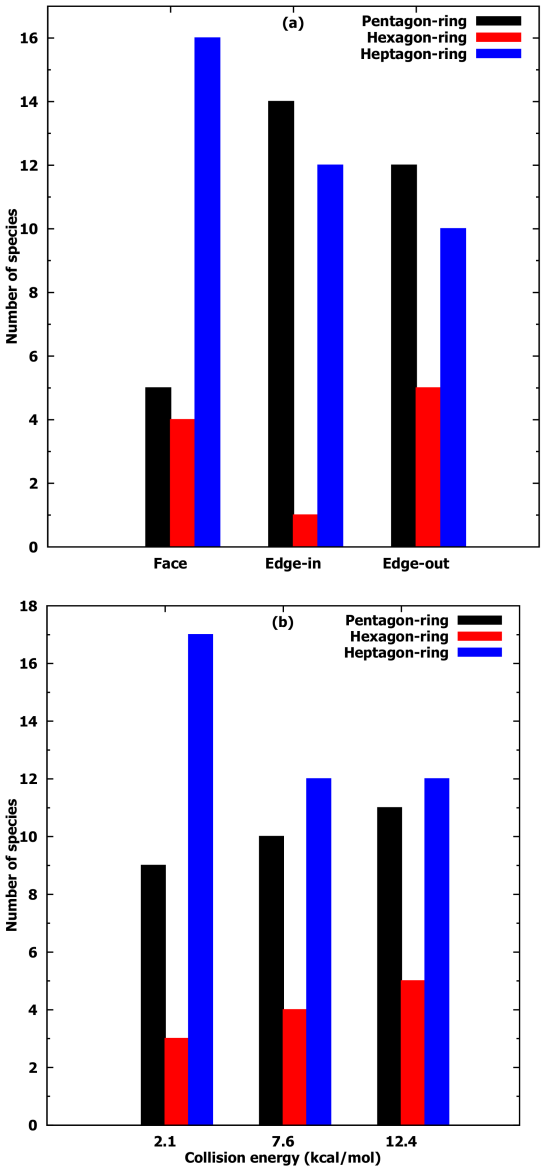

Fig. 4 Number of products resulting from CMB simulations at different collision directions (a) and collision energies (b) after 2 ps NVE QMMD simulations.

2. Reaction scheme of $C^+(^2P_J) + C_6H_6$ system

As Fig. 5 demonstrates, there are many pathways for the formation of the pentagon, hexagon and heptagon products, some of which are more frequently observed in the trajectories. For example, the R → Com-0 → P5, R→ P2 → P1 and R → Com-1 → P2 pathways are the most common routes in the production of pentagon, hexagon and heptagon series, respectively. They are all produced through complexes Com-0, Com-1 and Com-2, as observed over the simulations (Fig. 5). In fact, the positively charged carbon ion is a very strong electrophilic moiety that easily attacks the benzene π system. This way, it forms Com-0, Com-1 and Com-2 complexes with no barrier, exothermically by 155.2, 126.7

and 145.8 kcal mol^{-1}, respectively. All of these complexes are metastable and therefore they immediately undergo secondary reactions to yield more stable molecular ions. Accordingly, Com-0 will mainly eject two CH group producing polycycles with pentagons, while Com-1 and Com-2 may insert the carbon atom into the C-C bond yielding P2. In many cases, P2 remains stable on the MD time scale. Sometimes, however, it converts to P1 passing through TS7 (Fig. 7). The hexagon product, P1, is normally formed in this pathway. In a few cases, it is produced through Com-2, ejecting a CH group out of the ring.

According to earlier reports,[33, 34] the final molecules we observe in our simulations are actually intermediates and must undergo hydrogen dissociation reactions. These dissociation reactions may proceed by two mechanisms, i.e., electron recombination hydrogen dissociation (neutral path) or hydrogen dissociation (ionic path).[33] As shown in Fig. 5, in all cases the neutral pathway is more exothermic than the ionic path. Clearly, adding an electron into a positively ionic system releases energy resulting in the extra exothermicity of the neutral mechanism. In addition, as shown in Fig. 5 the most stable final product is P10-1 which is only observed in our simulations at a collision energy of 12.4 kcal mol^{-1}.

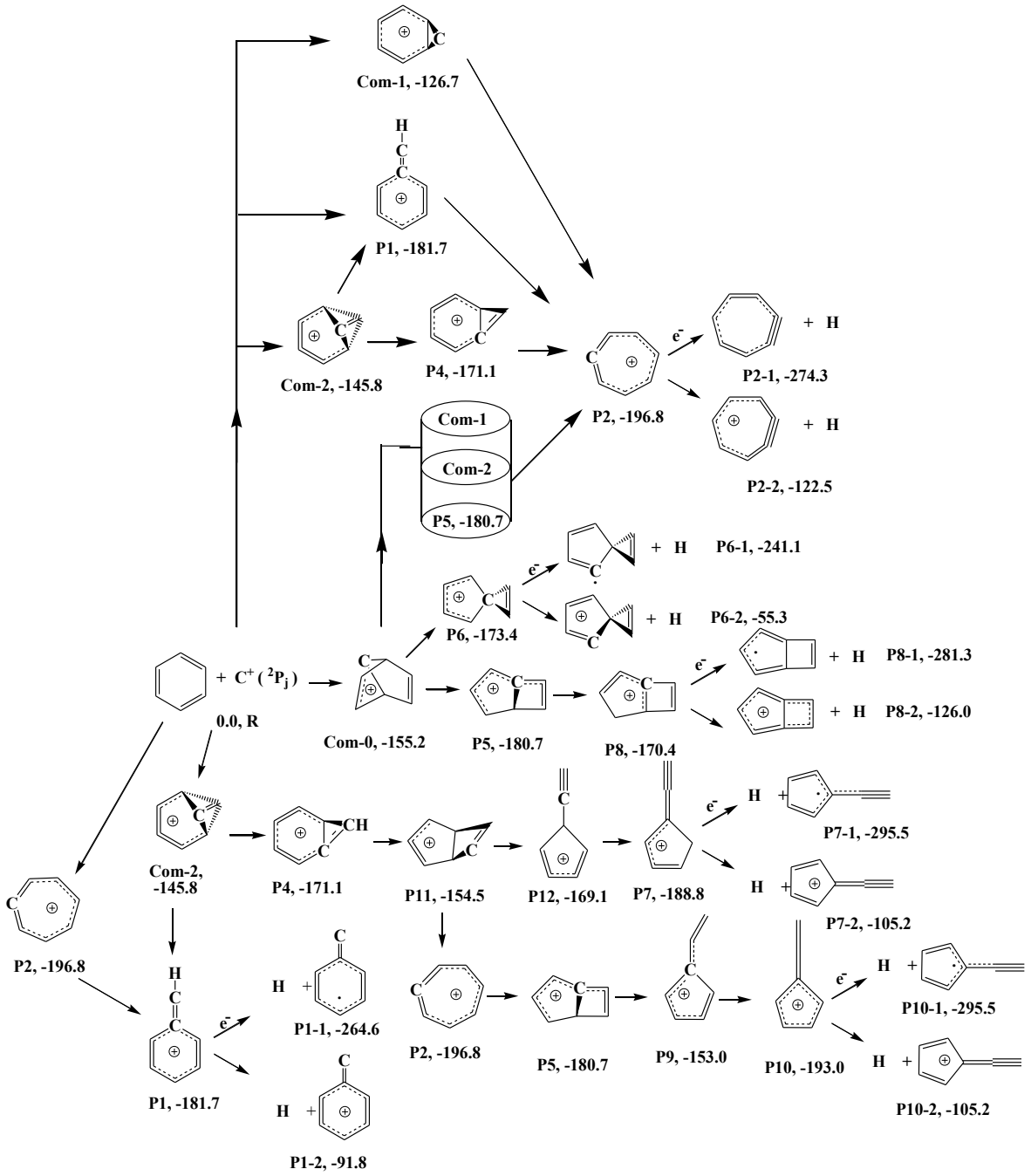

Fig. 5 Reaction scheme of $C^+(^2P_J)$ + C_6H_6 system based on our QMMD CMB simulations. All structures are in doublet state using PBE0-D3(BJ)/aug-cc-pVTZ + ZPVE (PBE0-D3(BJ)/aug-cc-pVTZ) level of theory. All energies are reported in kcal mol^{-1} and they are relative to the separated reactant energy.

2.1. Pentagon production pathways

As shown in Fig. 5, there are several isomers of pentagon products. The order of stability is P10, P7, P5, P6, P8 and Com-0. Although P10 and P7 are energetically the most stable, they were observed only

once and twice in the simulations, respectively. This is because they are formed from Com-2 and four/five barriers must be crossed to yield P7/P10. Moreover, Com-2 more likely forms P2 rather than P10 or P7, since they all have the same initial paths (up to TS7 for P10 & P2; up to P4 for P7 & P2), while TS7 directly converts to P2 which is also more stable than P10 or P7. Hence having fewer steps, fewer barriers, and high stability of P2, Com-2 is more likely to generate P2 rather than P10 or P7. Thus highly elusive intermediate P10 was only observed at the highest collision energy and P7 was produced solely from impacts with E_C= 7.6 kcal mol^{-1}.

In the production of pentagons, Com-0 mainly converts to P5 by passing TS1 (11.2 kcal mol^{-1} barrier height), which can happen at all collision energies. However, only at the highest collision energy, 12.4 kcal mol^{-1}, trajectories starting in P5 can pass a hydrogen migration barrier of 29.8 kcal mol^{-1} to give P8. In a few cases at E_C= 7.6 or 12.4 kcal mol^{-1}, pathways along TS1 generate P6 molecular ion. Therefore, the major product in the pentagon series is P5 and via hydrogen dissociation reactions, both the neutral and ionic routes, it could generate P8-1 or P8-2 directly.

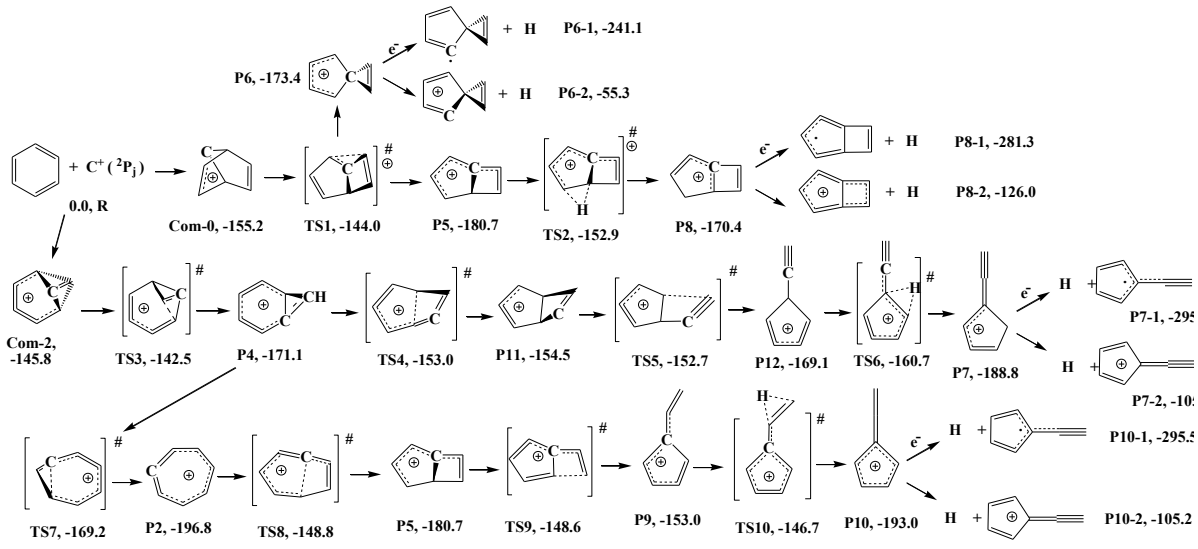

Fig. 6 Reaction scheme of the $C^+(^2P_J)$ + C_6H_6 system producing pentagons. All energies, reported in kcal mol^{-1}, are based on geometry optimization using PBE0-D3(BJ)/aug-cc-pVTZ + ZPVE (PBE0-D3(BJ)/aug-cc-pVTZ) level of theory and they are relative to the separated reactants.

2.2. Hexagon production pathways

The reaction scheme of hexagon production is shown in Fig. 7. As shown there are two paths yielding P1. The R → P2 → P1 pathway is the main path at all collision energies. By producing P2 a significant amount of energy is released (196.8 kcal mol^{-1}) and this energy is enough for the system to pass over TS7, which has a barrier height of 27.6 kcal mol^{-1}, to yield P1. P1 production through Com-2 is observed only for a few cases of E_C= 7.6 kcal mol^{-1}. Although we could not locate a TS along the R → Com-2

→ P1 pathway, there remains a competitive route R → Com-2 → P4 → P2 (Fig. 8) with very small energy barriers of 3.3 (TS13) and 1.9 (TS7) kcal mol^{-1}. Therefore, the system can pass these barriers easily at all collision energies and form P2 which is more stable than P1. Therefore, Com-2 predominantly reacts through the R → Com-2 → P4 → P2 pathway rather than following the R → Com-2 → P1 route. On the other hand, in contrast to the $C(^3P_J) + C_6H_6$ system, C-insertion in a C-H bond is very unlikely in the $C^+(^2P_J) + C_6H_6$ system. This insertion was observed only for 2 impacts out of 90 simulations, where it leads to P2 instead of P1 (Fig. 8).

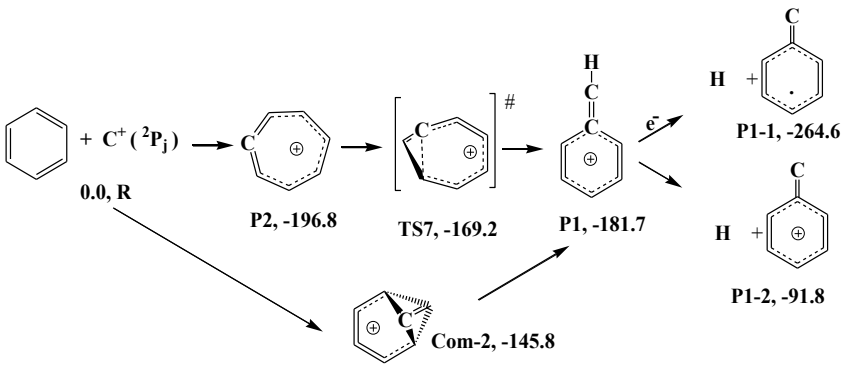

Fig. 7 Reaction scheme of hexagon production resulting from intermediates and TSes observed during CMB simulations of the $C^+(^2P_J) + C_6H_6$ system. Relative energies and structures are obtained from geometry optimization using PBE0-D3(BJ)/aug-cc-pVTZ + ZPVE (PBE0-D3(BJ)/aug-cc-pVTZ) level of theory.

2.3. Heptagon production pathways

As shown in Fig. 8, there remain seven pathways towards heptagon products, two of which are barrierless routes, R → Com-1 → P2 and R → Com-0 → Com-1 → P2. Accordingly, P2 is mainly produced from the Com-1 complex by the R → Com-1 → P2 pathway. The second major pathway is R → Com-2 → P4 → P2 along two tiny energy barriers of 3.3 (TS13) and 1.9 (TS7) kcal mol^{-1} (as discussed earlier) which are easy cross at all impact energies. At E_C=12.4 kcal mol^{-1}, Com-2 directly isomerizes to P1 and then by crossing a 25.1 kcal mol^{-1} barrier (through TS12), P2 is produced. The high barrier explains why this route was not observed at lower collision energies.

Only in two cases the carbon ion is inserted in a C-H bond via TS11 to form P1, and then yield P2 by passing TS12. Compared to the Com-1 and Com-2 pathways, Com-0 has a limited contribution to the production of the P2 molecular ion. Only one impact with 7.6 kcal mol^{-1} collision energy lead to the R → Com-0 → P5 → P2 pathway to form the heptagon product. Moreover, in a few cases, Com-0 converts to Com-1 or Com-2 isomerizing finally to the P2 product.

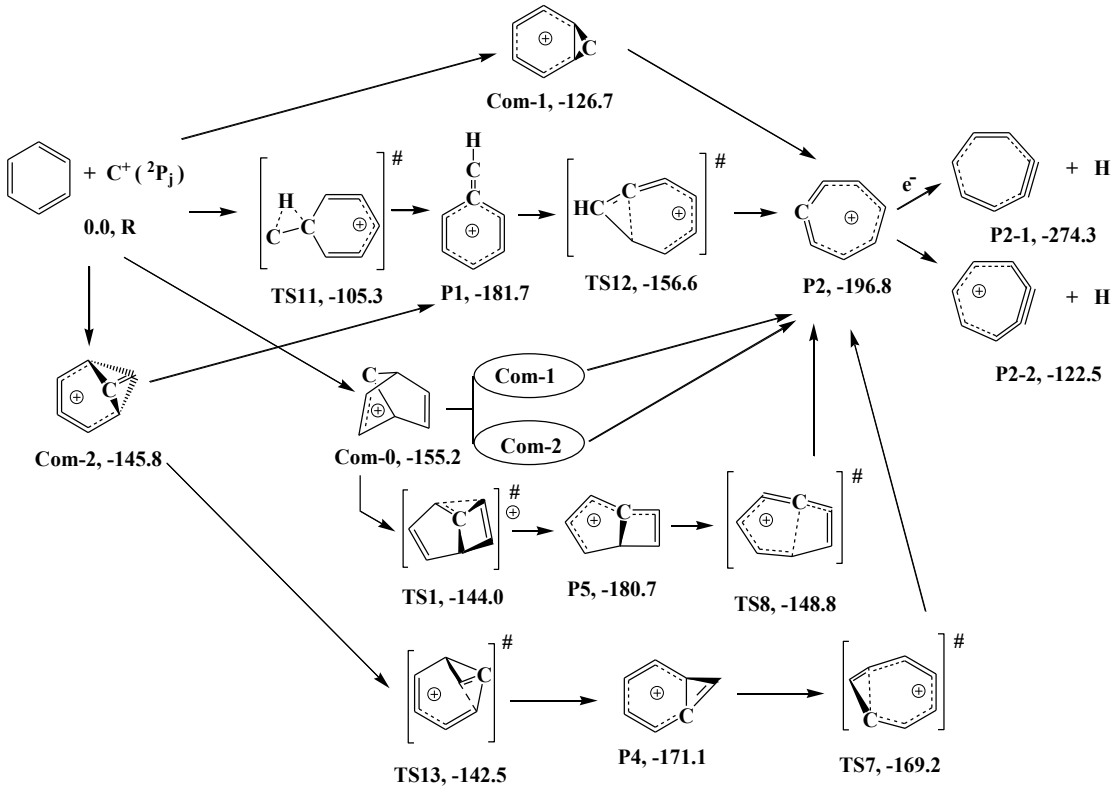

Fig. 8 Reaction scheme of heptagon production in our CMB simulations of the $C^+(^2P_J) + C_6H_6$ system. All energies are relative to the separated reactants and all structures are optimized at the PBE0-D3(BJ)/aug-cc-pVTZ + ZPVE (PBE0-D3(BJ)/aug-cc-pVTZ) level of theory.

C. Comparing the behavior of both systems

Except for charge and multiplicity, all simulation parameters were the same for both investigated systems. This allows for a rational comparison of the reactivity of the C atom and the C^+ ion. In the simulated trajectories, C^+ experiences a stronger attraction when it approaches the π-system of the benzene molecule in face and edge out-of-plane collisions. This is likely because of the positive charge and larger electron deficiency of the ion. In the edge-in-plane case, however, C^+ is strongly repelled by the partial positive charge on the hydrogen atoms. As a result, the benzene molecule rotates, the C^+ collides upon approaching from a new direction, and C^+ insertion in the C-H bond is avoided. Because of the lesser repulsion between neutral C and H, C atoms may insert in the C-H bond and produce P4 (Fig. 3). Indeed, this mechanism is the second most likely route in the $C(^3P_J) + C_6H_6$ system, while it only scarcely happens in the positively charged system.

As can be seen in Fig. 3 and Fig. 5, the chemical reactions of the charged system are much more exothermic in comparison to the neutral system. This surplus in energy can be converted into kinetic energy as depicted in Fig 9. This Figure shows the average kinetic energy over the simulations yielding heptagon-ring products, $C_7H_6/C_7H_6^+$, at E_C = 2.1 kcal mol^{-1}. This additional kinetic energy will in turn

facilitate more and different chemical reactions with higher barriers. Therefore, the reaction network in the charged system is considerably more complex. While the chemistry of the $C(^3P_J) + C_6H_6$ system is already quite well understood, insights into the $C^+(^2P_j) + C_6H_6$ system are scarce. The multitude of pathways, intermediates, products and transition states—many of which are not quite as intuitive—have hampered a comprehensive understanding. For this reason, a QMMD-based approach, as used here, has turned out to be a powerful tool. Explicit simulation of CMB experiments provides an unbiased way to probe the most relevant reaction mechanisms in this system, while fully taking into account the effect of released reaction heats in the isolated molecule.

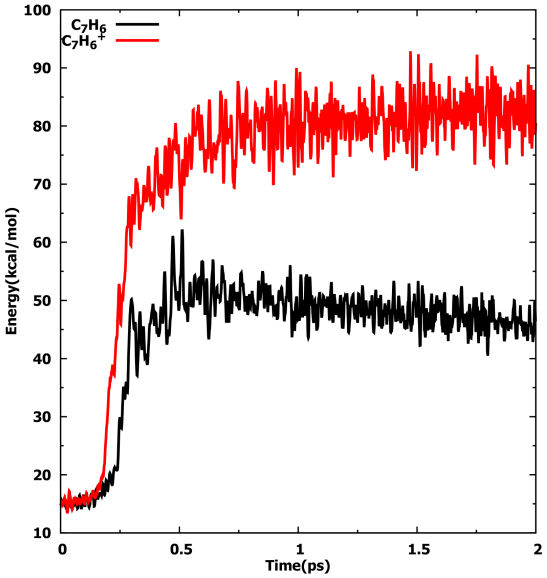

Fig. 9 Evolution of the average kinetic energy (in kcal mol^{-1}) versus time (ps) for the CMB simulations at E_C= 2.1 kcal mol^{-1} for two different impacts. The products are C_7H_6 and $C_7H_6^+$ resulting from the $C(^3P_J) + C_6H_6$ and $C^+(^2P_J) + C_6H_6$ collisions, respectively.

IV. Conclusions

In this study crossed molecular beam (CMB) experiments of $C(^3P_J) + C_6H_6$ and $C^+(^2P_J) + C_6H_6$ systems were simulated using quantum mechanical molecular dynamics (QMMD). The dynamic simulations were supplemented by static electronic structure calculations to derive an accurate reaction network and to elucidate the mechanisms of the reactions observed in the simulations. Comparing our results with the literature data shows that current method can accurately simulate the CMB of $C(^3P_J) + C_6H_6$ system. In fact, it was observed exactly the same products as reported earlier along with the reaction schemes that not only agree with the ones in the literature but also suggest new paths that are less likely to be

detected by experiments. Moreover, it was observed that the orientation of the collisions strongly affects the type of the final product, more so than the collision energy. This is because the energy release upon the initial collision is much higher larger than any of the barrier heights of the key subsequent reaction, making pathway selectivity mostly dictated by geometric factors. These insights are obtained from the QMMD simulations and may help in a better understanding of the reaction mechanisms, but would be very difficult to derive using experimental techniques only.

Many products are possible in the $C^+(^2P_J)$ + C_6H_6 system, making it far more complicated than the former. Therefore, experimental investigation of this system has been proven to be difficult. Using the QMMD method, three main series of products including pentagon, hexagon and heptagon molecular ions were identified. In each case, for each series, there are several paths leading to different isomers. This application to a challenging system shows the power of the QMMD method in supporting experimental techniques. The many isomers and pathways found for the $C^+(^2P_J)$ + C_6H_6 system demonstrates its ability to make predictions regarding chemical reactions taking place in interstellar media.

While our current study is limited to the reaction of benzene with carbon atoms and ions in a small range of conditions, it already demonstrates the ways in which QMMD simulation can deepen our understanding of chemical processes in interstellar media. Future studies could therefore be designed to extend the approach to different temperature and density regimes, and different chemical species. This way, it will be possible to address specific chemical questions that may arise in different interstellar environments.

Supplementary material

A video file of the simulations is provided Also, the results of the 30 extra simulations have been reported in the Table S1.

Conflicts of interest

There are no conflicts of interest to declare.

Acknowledgement

The financial support from the Iran Ministry of Science, Research and Technology and PLASMANT Research Group University of Antwerp is highly acknowledged by the authors. K.M.B. was funded as a junior postdoctoral fellow of the FWO (Research Foundation – Flanders), Grant 12ZI420N. The computational resources and services used in this work were provided by the HPC core facility CalcUA of the Universiteit Antwerpen, and VSC (Flemish Supercomputer Center), funded by the FWO and the Flemish Government.

References

1. J. L. Weisman, A. Mattioda, T. J. Lee, D. M. Hudgins, L. J. Allamandola, C. W. Bauschlicher Jr and M. Head-Gordon, *Physical Chemistry Chemical Physics*, 2005, **7**.
2. D. Hudgins, C. Bauschlicher, L. Allamandola and J. J. T. J. o. P. C. A. Fetzer, *The Journal of Physical Chemistry A*, 2000, **104**, 3655-3669.
3. P. Ehrenfreund, *Science*, 1999, **283**, 1123-1124.
4. M. Frenklach, *Physical chemistry chemical Physics*, 2002, **4**, 2028-2037.
5. X. Gu, Y. Guo, A. M. Mebel and R. I. Kaiser, *Chemical Physics Letters*, 2007, **449**, 44-52.
6. B. M. Jones, F. Zhang, R. I. Kaiser, A. Jamal, A. M. Mebel, M. A. Cordiner and S. B. Charnley, *Proc Natl Acad Sci U S A*, 2011, **108**, 452-457.
7. R. I. Kaiser and A. M. Mebel, *International Reviews in Physical Chemistry*, 2010, **21**, 307-356.
8. T. P. Snow and A. N. Witt, *Science*, 1995, **270**, 1455-1460.
9. C. F. McKee, *Astron. Soc. Pac.*, 1995, **80**, 292.
10. K. M. Ferrière, *Reviews of Modern Physics*, 2001, **73**, 1031-1066.
11. T. P. Snow and B. J. McCall, *Annual Review of Astronomy and Astrophysics*, 2006, **44**, 367-414.
12. N. Indriolo and B. J. McCall, *Chem Soc Rev*, 2013, **42**, 7763-7773.
13. P. Solomon and W. J. T. A. J. Klemperer, *The Astrophysical Journal*, 1972, **178**, 389-422.
14. A. K. Lemmens, D. B. Rap, J. M. M. Thunnissen, B. Willemsen and A. M. Rijs, *Nat Commun*, 2020, **11**, 269.
15. I. Hahndorf, H. Y. Lee, A. M. Mebel, S. H. Lin, Y. T. Lee and R. I. Kaiser, *The Journal of Chemical Physics*, 2000, **113**, 9622-9636.
16. I. Hahndorf, Y. T. Lee, R. I. Kaiser, L. Vereecken, J. Peeters, H. F. Bettinger, P. R. Schreiner, P. v. R. Schleyer, W. D. Allen and H. F. Schaefer, *The Journal of Chemical Physics*, 2002, **116**, 3248-3262.
17. L. C. L. Huang, H. Y. Lee, A. M. Mebel, S. H. Lin, Y. T. Lee and R. I. Kaiser, *The Journal of Chemical Physics*, 2000, **113**, 9637-9648.
18. R. I. Kaiser, A. M. Mebel, A. H. H. Chang, S. H. Lin and Y. T. Lee, *The Journal of Chemical Physics*, 1999, **110**, 10330-10344.
19. R. I. Kaiser, D. S. Parker, F. Zhang, A. Landera, V. V. Kislov and A. M. Mebel, *J Phys Chem A*, 2012, **116**, 4248-4258.
20. A. M. Thomas, M. Lucas, L. Zhao, J. Liddiard, R. I. Kaiser and A. M. Mebel, *Phys Chem Chem Phys*, 2018, **20**, 10906-10925.
21. J. Hutter, M. Iannuzzi, F. Schiffmann and J. VandeVondele, *Wiley Interdisciplinary Reviews: Computational Molecular Science*, 2014, **4**, 15-25.
22. A. D. Becke, *J Chem Phys*, 2014, **140**, 18A301.
23. J. VandeVondele and J. Hutter, *J Chem Phys*, 2007, **127**, 114105.
24. T. D. Kühne, M. Iannuzzi, M. Del Ben, V. V. Rybkin, P. Seewald, F. Stein, T. Laino, R. Z. Khaliullin, O. Schütt, F. Schiffmann, D. Golze, J. Wilhelm, S. Chulkov, M. H. Bani-Hashemian, V. Weber, U. Borštnik, M. Taillefumier, A. S. Jakobovits, A. Lazzaro, H. Pabst, T. Müller, R. Schade, M. Guidon, S. Andermatt, N. Holmberg, G. K. Schenter, A. Hehn, A. Bussy, F. Belleflamme, G. Tabacchi, A. Glöß, M. Lass, I. Bethune, C. J. Mundy, C. Plessl, M. Watkins, J. VandeVondele, M. Krack and J. Hutter, *The Journal of Chemical Physics*, 2020, **152**.
25. C.-C. Ye, Q. An, T. Cheng, S. Zybin, S. Naserifar, X.-H. Ju and W. A. Goddard III, *Journal of Materials Chemistry A*, 2015, **3**, 12044-12050.
26. R. Berraud-Pache, C. Garcia-Iriepa and I. Navizet, *Frontiers in chemistry*, 2018, **6**, 116.
27. T. Zhou, T. Cheng, S. V. Zybin, W. A. Goddard III and F. J. J. o. M. C. A. Huang, 2018, **6**, 5082-5097.
28. N. Balucani, A. M. Mebel, Y. T. Lee and R. I. Kaiser, *The Journal of Physical Chemistry A*, 2001, **105**, 9813-9818.

29. Y. Guo, A. M. Mebel, F. Zhang, X. Gu and R. I. Kaiser, *J Phys Chem A*, 2007, **111**, 4914-4921.
30. T. Yang, L. Muzangwa, D. S. Parker, R. I. Kaiser and A. M. Mebel, *Phys Chem Chem Phys*, 2015, **17**, 530-540.
31. R. I. Kaiser, I. Hahndorf, L. C. L. Huang, Y. T. Lee, H. F. Bettinger, P. v. R. Schleyer, H. F. Schaefer and P. R. Schreiner, *The Journal of Chemical Physics*, 1999, **110**, 6091-6094.
32. R. Kaiser, O. Asvany and Y. Lee, *Planetary Space Science*, 2000, **48**, 483-492.
33. E. Herbst, *Chemical Society Reviews*, 2001, **30**, 168-176.
34. R. D. Smith and J. J. DeCorpo, *The Journal of Physical Chemistry A*, 1976, **80**, 2904-2910.
35. R. M. Lemon, *Accounts of Chemical Research*, 1973, **6**, 65-73.
36. F. Zhang, X. Gu and R. I. Kaiser, *J Chem Phys*, 2008, **128**, 084315.
37. X. Gu, Y. Guo, F. Zhang, A. M. Mebel and R. I. Kaiser, *Chemical Physics Letters*, 2007, **436**, 7-14.
38. X. Gu, F. Zhang, Y. Guo and R. I. Kaiser, *Angew Chem Int Ed Engl*, 2007, **46**, 6866-6869.
39. A. M. Mebel and R. I. Kaiser, *International Reviews in Physical Chemistry*, 2015, **34**, 461-514.
40. R. I. Kaiser, O. Asvany, Y. T. Lee, H. F. Bettinger, P. v. R. Schleyer and H. F. Schaefer, *The Journal of Chemical Physics*, 2000, **112**, 4994-5001.
41. Y. Guo, X. Gu, E. Kawamura and R. I. Kaiser, *Review of Scientific Instruments*, 2006, **77**.
42. T. E. Markland and M. Ceriotti, *Nature Reviews Chemistry*, 2018, **2**, 0109.
43. P. M. Woods, T. J. Millar, A. A. Zijlstra and E. Herbst, *The Astrophysical Journal*, 2002, **574**, L167-L170.
44. J. Cernicharo, A. M. Heras, A. G. G. M. Tielens, J. R. Pardo, F. Herpin, M. Guélin and L. B. F. M. Waters, *The Astrophysical Journal*, 2001, **546**, L123-L126.
45. J. VandeVondele, M. Krack, F. Mohamed, M. Parrinello, T. Chassaing and J. Hutter, *Computer Physics Communications*, 2005, **167**, 103-128.
46. B. G. Lippert, J. H. Parrinello and Michele, *Molecular Physics*, 2010, **92**, 477-488.
47. S. Goedecker, M. Teter and J. Hutter, *Physical Review B*, 1996, **54**, 1703.
48. M. Krack, *Theoretical Chemistry Accounts*, 2005, **114**, 145-152.
49. M. Ernzerhof and G. E. Scuseria, *The Journal of chemical physics*, 1999, **110**, 5029-5036.
50. C. Adamo and V. Barone, *The Journal of chemical physics*, 1999, **110**, 6158-6170.
51. S. Grimme, J. Antony, S. Ehrlich and H. Krieg, *The Journal of chemical physics*, 2010, **132**, 154104.
52. S. Grimme, S. Ehrlich and L. Goerigk, *Journal of computational chemistry*, 2011, **32**, 1456-1465.
53. L. Goerigk, A. Hansen, C. Bauer, S. Ehrlich, A. Najibi and S. Grimme, *Phys Chem Chem Phys*, 2017, **19**, 32184-32215.
54. J. P. Perdew, K. Burke and M. Ernzerhof, *Physical review letters*, 1996, **77**, 3865.
55. R. Peverati, *International Journal of Quantum Chemistry*, 2020.
56. M. Guidon, J. Hutter, J. VandeVondele and computation, *Journal of chemical theory*, 2010, **6**, 2348-2364.
57. G. W. T. A. Frisch, H. B. Schlegel, G. E. Scuseria, M. A. Robb, J. R. Cheeseman, G. Scalmani, V. Barone, B. Mennucci, G. A. Petersson, H. Nakatsuji, M. Caricato, X. Li, H. P. Hratchian, A. F. Izmaylov, J. Bloino, G. Zheng, J. L. Sonnenberg, M. Hada, M. Ehara, K. Toyota, R. Fukuda, J. Hasegawa, M. Ishida, T. Nakajima, Y. Honda, O. Kitao, H. Nakai, T. Vreven, J. A. Montgomery, J. E. Peralta, F. Ogliaro, M. Bearpark, J. J. Heyd, E. Brothers, K. N. Kudin, V. N. Staroverov, R. Kobayashi, J. Normand, K. Raghavachari, A. Rendell, J. C. Burant, S. S. Iyengar, J. Tomasi, M. Cossi, N. Rega, J. M. Millam, M. Klene, J. E. Knox, J. B. Cross, V. Bakken, C. Adamo, J. Jaramillo, R. Gomperts, R. E. Stratmann, O. Yazyev, A. J. Austin, R. Cammi, C. Pomelli, J. W. Ochterski, R. L. Martin, K. Morokuma, V. G. Zakrzewski, G. A. Voth, P. Salvador, J. J. Dannenberg, S. Dapprich, A. D. Daniels, Ö. Farkas, J. B. Foresman, J. V. Ortiz, J. Cioslowski, D. J. Fox and I. Gaussian, Wallingford CT, 2009.
58. T. H. Dunning Jr, *The Journal of chemical physics*, 1989, **90**, 1007-1023.

59. H. B. Schlegel, *Journal of Computational Chemistry*, 1982, **3**, 214-218.